A multi-detector experimental setup for the study of space radiation shielding materials: Measurement of secondary radiation behind thick shielding and assessment of its radiobiological effect

Felix Horst[1], *Daria* Boscolo[1], *Giorgio* Cartechini[2,3], *Marco* Durante[1,4], *Carola* Hartel[1], *Ekaterina* Kozlova[1], *Chiara* La Tessa[2,3], *Marta* Missiaggia[2,3], *Enrico* Pierobon[2,3], *Torsten* Radon[1], *Riccardo* Ridolfi[5,6], *Sylvia* Ritter[1], *Christoph* Schuy[1], *Alexey* Sokolov[1], *Uli* Weber[1], *Miroslav* Zbořil[7*]

[1]GSI Helmholtzzentrum für Schwerionenforschung Darmstadt, Planckstraße 1, 64291 Darmstadt, Germany
[2]Trento Institute for Fundamental Physics and Applications – Istituto Nazionale di Fisica Nucleare (TIFPA-INFN), Via Sommarive 14, 38122 Trento, Italy
[3]University of Trento, Via Sommarive 14, 38123 Trento, Italy
[4]Technical University of Darmstadt, Institute for Condensed Matter Physics, Hochschulstr. 6, 64289 Darmstadt, Germany
[5]Istituto Nazionale di Fisica Nucleare (INFN), Section of Bologna, Viale Berti Pichat 6/2, 40127 Bologna, Italy
[6]University of Bologna, Department of Physics and Astronomy, Viale Berti Pichat 6/2, 40127 Bologna, Italy
[7]Physikalisch-Technische Bundesanstalt (PTB), Bundesallee 100, 38116 Braunschweig, Germany

Abstract. Space agencies have recognized the risks of astronauts' exposure to space radiation and are developing complex model-based risk mitigation strategies. In the foundation of these models, there are still significant gaps of knowledge concerning nuclear fragmentation reactions which need to be addressed by ground-based experiments. There is a lack of data on neutron and light ion production by heavy ions, which are an important component of galactic cosmic radiation (GCR). A research collaboration has been set up to characterize the secondary radiation field produced by GCR-like radiation provided by a particle accelerator in thick shielding. The aim is to develop a novel method for producing high-quality experimental data on neutron and light ion production in shielding materials relevant for space radiation protection. Four complementary detector systems are used to determine the energy and angular distributions of high-energy secondary neutrons and light ions. In addition to the physical measurement approach, the biological effectiveness of the secondary radiation field is determined by measuring chromosome aberrations in human peripheral lymphocytes placed behind the shielding. The experiments are performed at the heavy ion

* Corresponding author: miroslav.zboril@ptb.de

synchrotron SIS18 at the GSI Helmholtzzentrum für Schwerionenforschung in Darmstadt, Germany, in the frame of FAIR Phase-0.

1 Motivation

The health effects of space radiation on astronauts represent a major limiting factor for long-duration human space missions beyond low Earth orbit [1]. The radiation exposure can potentially cause cancer and other late effects. National space agencies have recognized the risks related to exposure to space radiation and are developing complex model-based risk mitigation strategies [2, 3]. The space radiation risk models are based on interplay of radiation transport physics and radiobiology. In both fields, there are still significant gaps of knowledge which need to be closed by collecting high-quality experimental data and developing the corresponding theoretical models and simulation codes.

During passage through the shield, a major fraction of the heavy ions in the galactic cosmic radiation (GCR) break up due to nuclear fragmentation reactions into neutrons and light charged fragments. A relevant literature gap exists for neutron and light ion production in thick shielding upon the impact of GCR [4]. Due to their high penetration power and high biological effectiveness, neutrons represent a significant threat to the astronauts' health. The issue of neutron production in thick shielding is particularly important in design studies of habitats constructed from the local regolith, for instance for longer manned missions to the Moon or Mars surface. Recent comparisons of common particle transport codes used in the space radiation community (e.g., FLUKA, Geant4, MCNP, PHITS, HZETRN and SHIELD) suggest that differences in the neutron and light ion production models still cause significant discrepancies [2]. The reasons for that are uncertainties in the nuclear physics models describing the heavy ion total reaction cross sections [5] and the limited base of experimental double-differential cross sections [6].

To tackle these issues, a research collaboration has been set up to characterize the secondary radiation field produced by GCR-like radiation provided by a particle accelerator in thick shielding by means of a multi-detector setup consisting of complementary experimental systems. A cylindrical target is irradiated with a high-energy heavy ion beam and the various detectors, arranged around the target at defined angles, characterize different aspects of the secondary radiation field. The experiments at GSI Helmholtzzentrum für Schwerionenforschung in Darmstadt, Germany, are performed in the framework of the Investigations into Biological Effects of Radiation (IBER) program funded by the European Space Agency (ESA).

In the present article, the detection systems and their interplay are described. The different physical detector systems used are the Bonner sphere spectrometer NEMUS, an ambient dosimeter and a Bonner spectrometer based on thermoluminescence dosimetry (TLD), scintillator telescopes with time-of-flight (ToF) electronics and a tissue-equivalent proportional counter (TEPC). In addition, human blood lymphocytes are used as biological dosimeters. Based on the combination of these different methods, the secondary radiation field at the chosen angles of interest is well characterized. The quantities obtained with the different systems are neutron and light ion energy distributions, absorbed dose, ambient dose equivalent, microdosimetric spectra and the mean quality factor.

2 Experimental setups and methodology

A schematic of the experimental setup used during first experiments performed in Cave A at GSI with 1 GeV/u ^{56}Fe ions on a thick aluminum target is shown in Figure 1. As angles of interest 15° and 40° relative to the beam axis were chosen. As an example, the setup for

irradiation of the human blood lymphocytes with simultaneous measurements using TEPC detectors on the other side of the beam axis is shown. The primary 1 GeV/u ^{56}Fe ion beam exits the vacuum beam line through a thin exit window and penetrates a beam monitor ionization chamber. The beam intensity is adjusted to match the optimal measurement conditions of each detector system. Optionally, for low intensity measurements like during the ToF experiment, also a plastic scintillator can be inserted. The monitor ionization chamber can be calibrated in terms of number of primary particles either by an absolute absorbed dose to water measurement in a scanned field under defined reference conditions [7] or by comparison of the ionization current with the rate measured by the plastic scintillator. After passing the beam monitors, the primary ions are stopped in a thick aluminum target (20 cm diameter) and produce different secondary particle species. The most abundant secondary particles are neutrons and protons. As indicated in Fig. 1, the distance of the different systems from the target center can be chosen individually to adapt to specific dose rate requirements. The difference in distances to the target center can, in principle, lead to different neutron spectra due to different contributions of the room-return neutrons. For the first evaluation of the physical detectors' and biodosimetry results, this effect will be assessed by a dedicated Monte Carlo study.

Aluminum is a "standard material" for space radiation protection research as it is the main structural material in space crafts and was therefore chosen for the first measurement campaign. For future experiments it is intended to characterize other materials as well, for example Moon regolith which could be used for lunar habitats [8], and to use also other primary ion species than ^{56}Fe ions.

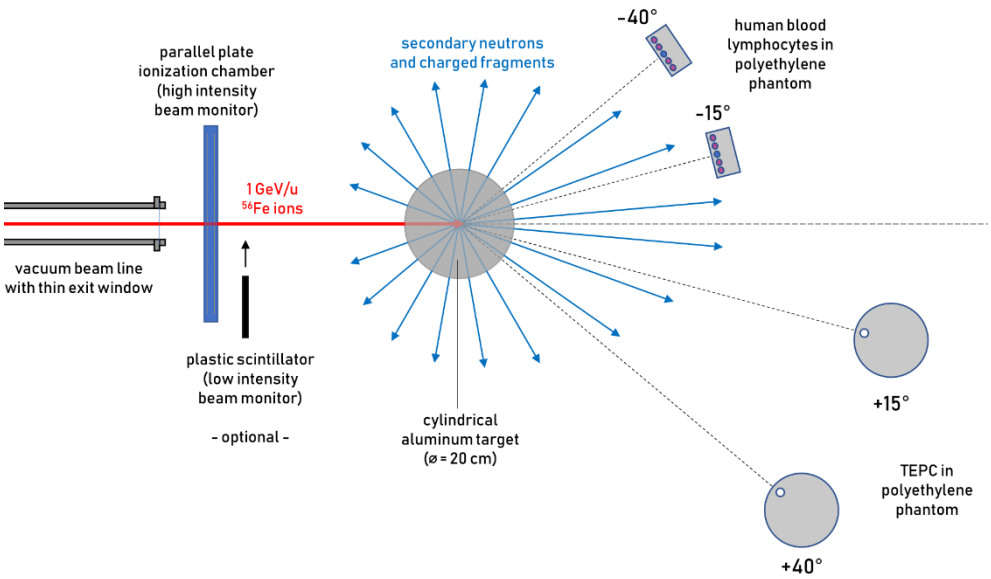

Fig. 1. Schematic of the multi-detector setup used for characterization of the secondary neutron and light ion radiation field produced by a high-energy heavy ion beam in a thick target.

In the following Sections, each experimental system used is described in more detail and the interplay of the different systems is depicted.

2.1 PTB Bonner sphere spectrometer NEMUS

A Bonner sphere spectrometer (BSS) is a commonly used detector system for the measurement of neutron energy distributions in unknown fields [9, 10]. A BSS consists of a set of moderating spheres with different diameters and a thermal neutron sensor that is placed at the center of each sphere. Each sphere plus thermal sensor combination has a different energy-dependent response to neutrons. The peak of the neutron response function shifts to higher neutron energies as the size of the moderator increases. It is common practice to measure also with the thermal neutron sensor without a moderating sphere (i.e., the bare detector).

In the framework of this project, the BSS NEMUS [11] developed at PTB in Braunschweig, Germany, is used. The BSS NEMUS is a secondary transfer standard of PTB, traceable to the primary standards of neutron fluence rate. It consists of ten polyethylene (PE) spheres with diameters ranging from 7.6 cm (3 inch) to 30.5 cm (12 inch). The set also contains a bare detector (diameter 3.2 cm), a Cd-covered detector, and four modified spheres with lead (Pb) and copper (Cu) shells. Thanks to these metal shells, embedded in the PE spheres, the response functions of the four modified spheres dramatically increase for neutron energies above 50 MeV. Typically, the central thermal neutron sensors (CTNS) are spherical ^{3}He-filled proportional counters (type SP9, company Centronic Ltd.), detecting the thermalized neutrons via the reaction ^{3}He(n,p)^{3}He with a Q value of 764 keV. For the measurements carried out at GSI, we use SP9 counters with ^{3}He pressure of 20 kPa and 200 kPa, respectively, to control the possible effects of dead time-caused signal losses. In addition, a ^{235}U-coated cylindrical fission chamber (type 307719, company LND, Inc.) is alternatively used as CTNS on certain measurement locations, to allow for a better discrimination of the neutron- and gamma-components of the secondary field behind the target. This is possible thanks to the neutron detection mechanism of the ^{235}U fission chamber (^{235}U(n,f)) with a large Q value of about 200 MeV. In addition, the thermal neutron detection efficiency of the specific ^{235}U fission chamber, used in this project, is by a factor of ~200 lower compared to the widely used ^{3}He-filled SP9 counter with 200 kPa filling pressure, which also improves the control on possible dead-time effects.

To cover the complete energy range of the expected neutron field and minimize the required measurement time, we chose a subset of NEMUS spheres, namely a bare counter, spheres of diameters of 7.6, 10.2, 12.7, 15.2, 20.3, 25.4 and 30.5 cm, respectively, plus all four modified spheres with metal shells. This way it is possible to cover the entire neutron energy spanning from the thermal neutrons up to the high-energy neutrons above 1 GeV. It should be noted, however, that the neutron response functions of the BSS NEMUS are validated in the PTB neutron reference fields only up to 20 MeV, and above this value the response functions rely purely on nuclear models implemented in the MCNP6 code. For quality-assurance reasons, the CTNS signals are recorded in a time-resolved manner. From the pulse-height spectra, the number of neutron-induced counts in each sphere is determined. This information is used in the unfolding process, together with the NEMUS response functions and an *a priori* (default) neutron energy distribution (spectrum) obtained from dedicated Monte Carlo simulations, to derive the resulting neutron spectrum.

2.2 TLD-based neutron ambient dosimeters and Bonner spectrometer

For neutron ambient dose measurements, the GSI ball neutron dosimeter [12] is used. This passive dosimeter, equipped with Harshaw TLD cards (one TLD-600H and one 700H pair), has a neutron response function close to fluence-to-ambient-dose conversion coefficients and, therefore, provides read-out values close to the ambient dose equivalent $H^*(10)$. First results for 1 GeV/u ^{56}Fe ions on a thick aluminum target have been published [13] and the

dosimeter $H^*(10)$ readings were comparable with the predictions by the Monte Carlo code FLUKA.

Furthermore, a BSS-like spectrometer set based on the same TLD cards, consisting of one PE box ($2 \times 5 \times 7$ cm³), one PE cylinder (diameter: 5.1 cm, height: 6 cm), four PE spheres (diameters of 12.7, 20.3, 25.4 and 30.5 cm, respectively), one PE sphere (diameter of 32.5 cm) with a 1 cm thick lead layer as well as one polyvinyl chloride (PVC) cylinder (height and diameter: 14 cm), also with additional lead and PE layers, is used for neutron spectrometry. For this purpose, the elements of the set are irradiated one after another at a certain position and the spectrum is unfolded from the readouts using the GRAVEL [14] unfolding program. First results for 1 GeV/u ^{56}Fe ions on aluminum have been published as well [15] and as for $H^*(10)$, also the measured neutron spectra are in reasonably good agreement with FLUKA calculations.

2.3 Time-of-flight spectrometry using scintillator telescopes

Another common method for measuring spectra of high-energy neutrons and charged fragments produced in heavy ion reactions is time-of-flight (ToF) spectrometry, where scintillators or combinations of scintillators ("scintillator telescopes") are used as particle detectors and to discriminate between different particle types [16]. The time between the heavy ions hitting the target and the particles arriving at the detector is recorded in event-by-event mode. From the time-of-flight of the single particles, velocity distributions are obtained which can then be converted into energy spectra of secondary neutrons and charged fragments (protons, deuterons, tritons, ^{3}He, ^{4}He, etc.).

While for charged particles, scintillators have practically a 100 % detection efficiency, the neutron efficiency that is reached for common scintillator materials and geometries is typically not higher than 15 %, depending, however, on the specific scintillator thickness. The neutron efficiency of a scintillator is usually a function of energy and this has to be taken into account to obtain absolute neutron spectra from such a measurement [17]. The lowest neutron energy that can be detected by the ToF method is around 10 MeV with common experimental electronics, therefore only the high-energy part of a neutron spectrum is determined.

2.4 Tissue-equivalent proportional counter

The distribution of energy deposition on a micrometer scale as relevant for mechanistic understanding of radiobiological effects can be measured with a tissue-equivalent proportional counter (TEPC). The microdosimetric quantities obtained in such a measurement are spectra of specific energy and lineal energy, the equivalents to the macroscopic quantities absorbed dose and linear energy transfer (LET).

The TEPC used in the experiments described in this article is the model LET-1/2 from the company Far West Technology. The TEPC detector is placed at 1 cm depth within a polyethylene phantom (see Fig. 1) to be consistent with the $H^*(10)$ measurements performed with TLDs and the irradiation of blood lymphocytes at the same depth. It is operated with a voltage of 700 V and read out by a charge-sensitive preamplifier (model A422A from CAEN). As the TEPC signals can span several orders of magnitude, they are fed into three different shaping amplifiers: two of model N968 from CAEN with gains of 100 and 1000, and one of model 7243E by Intertechnique with a gain of 10. Finally, the amplified signals are recorded by multichannel analyzers (models 926/927 from ORTEC). The three recorded spectra are overlapping so that they can be merged together in an offline analysis step.

The obtained microdosimetric spectra can then be analyzed to assess the radiation quality [18, 19].

2.5 Chromosome aberrations in human blood lymphocytes (biodosimetry)

All detector systems described above are physical detectors. A complementary approach to assess the biological effect of a radiation exposure is the so-called cytogenetic biodosimetry, i.e., the analysis of chromosome aberrations in human peripheral blood lymphocytes. Chromosome aberrations are a sensitive indicator of an exposure to ionizing radiation and provide information on radiation-associated health risks, in particular the risk of cancer induction [20]. In the scope of space radiation protection, a comparable approach using human fibroblasts was presented by Slaba *et al.* [21].

Within this project, biodosimetry is performed with human peripheral blood lymphocytes following standard techniques [22]. Blood is taken from a healthy donor. Then, the lymphocytes are isolated, transferred into plastic tubes and placed at a depth of 1 cm within a polyethylene phantom. Samples are irradiated with doses from about 100 mGy up to 1 Gy. The absorbed dose is measured using a PTW 30013 Farmer ionization chamber that is placed in the phantom next to the cell samples, enabling a direct comparison of biological effects and physical dose. After exposure, the cytogenetic damage is analyzed in lymphocytes at the first post-irradiation mitosis. As the difference in the energy deposition of high- and low-LET radiation does not only affect the number of aberrations produced per unit dose, but also the types of aberrations, the high-resolution 24-color karyotyping technique (multiplex fluorescence *in situ* hybridization, mFISH) is applied. This method allows, for example, to visualize complex chromosome exchanges that are a signature of high-LET radiation [23, 24]. As previous measurements were mostly done with fission neutrons [25] and there are hardly any high-resolution data for high-energy neutrons as produced by GCR, the presented experiments are expected to fill this gap.

The irradiations are performed with high beam intensity to reach doses above 100 mGy in the scattered radiation field behind the target within a reasonable time (i.e., a few hours). Taking into account that the dose rate under these irradiation conditions is rather low (a few mGy/min), dose-effect curves for the induction of aberrations in lymphocytes by 220 kV X-rays (i.e., the reference radiation) at a comparable dose rate will be measured as well.

3 Interplay between experimental setups

The presented multi-detector approach allows a very accurate characterization of the secondary radiation fields studied. The single systems suffer from different issues; however, these can be overcome by combining the different measurements that complement each other in that sense. For instance, some of the Bonner spectrometer elements, both in the NEMUS setup and in the TLD-based system, respond not only to neutrons but also to high-energy protons and other charged fragments. Therefore, information about the secondary charged fragment spectra is required to correct the detector readings, and this is available from the scintillator ToF measurements.

With the ToF spectrometry, it is possible to determine the neutron spectra only above 10 MeV, while the energy distribution of the secondary neutrons is continuous and extends down to thermal neutron energies. With the Bonner spectrometry methods, the entire neutron spectra are determined, but with lower resolution at high energies. Therefore, overlapping the neutron spectra obtained by ToF and Bonner spectrometry can give a more accurate measurement of the neutron spectra than both methods alone. In addition, the absolute scale of the neutron energy distributions, resulting from the analysis of ToF, BSS NEMUS and TLD-based BSS, will be systematically compared to achieve a unified assessment of the absolute secondary neutron production yields.

Neutrons show an increased radiobiological effectiveness, i.e., a larger biological effect (e.g., induce more chromosome aberrations [25]) compared to low-LET reference radiation

at the same absorbed dose level. This higher relative biological effectiveness (RBE) is due to the secondary particles (mostly recoil protons) generated by neutrons when interacting with tissue. The magnitude of these effects depends strongly on the neutron energy spectrum as well as on the tissue type, dose and dose rate. In radiation protection, the maximum RBE for oncogenic transformations of a given radiation field is approximated by so-called quality factors Q. The International Commission on Radiological Protection (ICRP) has defined a function which describes the dependence of the quality factor Q on the LET [26] which can also be applied to neutrons if the LET spectrum of their secondary particles is known [27]. The absorbed dose D multiplied with Q gives the dose equivalent H which can serve as a measure for the late risk associated with a radiation exposure. The lineal energy spectra obtained with the TEPC detector are a good proxy for the LET spectra and can be used to calculate the mean quality factor using the ICRP function. The absorbed dose D is directly measured with Farmer ionization chambers during irradiation of the biological samples and the neutron dose equivalent H is measured by the TLD-based ambient dosimeters. From these two quantities, the mean quality factor can be calculated as well. The RBE values, obtained from the biodosimetry, will be compared to the quality factors obtained by physical dosimetry, to understand how reliably the quality factors, used in radiation protection practice, can actually estimate the biological effectiveness of mixed radiation fields with a high neutron component induced by GCR-like heavy ions in thick shielding, as relevant for space radiation protection.

4 Summary and Outlook

A multi-detector setup for characterization of secondary neutron and light ion fields, produced by GCR-like heavy ions, which is of interest for the field of space radiation protection, was presented. The different experimental methods were described, and their interplay was outlined.

First experiments with 1 GeV/u ^{56}Fe ions on a thick aluminum target have been carried out in Cave A at GSI Helmholtzzentrum für Schwerionenforschung in Darmstadt, Germany, in the framework of the IBER program funded by ESA. The results obtained with the TLD-based detector systems are already published [13, 15] and the measurement data from the other methods are currently being analyzed.

Future experiments will also study different materials like Moon regolith and other primary ion species.

This experiment is performed at the heavy ion synchrotron SIS18 at the GSI Helmholtzzentrum für Schwerionenforschung, Darmstadt (Germany) in the frame of FAIR Phase-0. The beam time is funded by the European Space Agency (ESA) in the framework of the IBER project. This experiment is funded by the German Space Agency at the German Aerospace Center (DLR) under the funding number 50WB2125. The authors would like to thank M. Dommert, T. Klages, A. Lücke, M. Reginatto and A. Zimbal from PTB Braunschweig for fruitful cooperation.

References

1. M. Durante, Life Sciences in Space Research **1**, 2 (2014)
2. J.W. Norbury, T.C. Slaba, S. Aghara, F.F. Badavi, S.R. Blattnig, M.S. Clowdsley, L.H. Heilbronn, K. Lee, K.M. Maung, C.J. Mertens, J. Miller, R.B. Norman, C.A. Sandridge, R. Singleterry, N. Sobolevsky, J.L. Spangler, L.W. Townsend, C.M. Werneth, K. Whitman, J.W. Wilson, S.X. Xu, C. Zeitlin, Life Sciences in Space Research **22**, 98 (2019)

3. L. Walsh, U. Schneider, A. Fogtman, C. Kausch, S. McKenna-Lawlor, L. Narici, J. Ngo-Anh, G. Reitz, L. Sabatier, G. Santin, L. Sihver, U. Straube, U. Weber, M. Durante, Life Sciences in Space Research **21**, 73 (2019)
4. J.W. Norbury, T.C. Slaba, Life Sciences in Space Research **3**, 90 (2014)
5. F. Luoni, F. Horst, C.A. Reidel, A. Quarz, L. Bagnale, L. Sihver, U. Weber, R.B. Norman, W. de Wet, M. Giraudo, G. Santin, J.W. Norbury, M. Durante, New J. Phys. **23**, 101201 (2021)
6. J.W. Norbury, G. Battistoni, J. Besuglow, L. Bocchini, D. Boscolo, A. Botvina, M. Clowdsley, W. de Wet, M. Durante, M. Giraudo, T. Haberer, L. Heilbronn, F. Horst, M. Krämer, C. La Tessa, F. Luoni, A. Mairani, S. Muraro, R.B. Norman, V. Patera, G. Santin, C. Schuy, L. Sihver, T.C. Slaba, N. Sobolevsky, A. Topi, U. Weber, C.M. Werneth, C. Zeitlin, Frontiers in Physics **8**, 565954 (2020)
7. F. Luoni, U. Weber, D. Boscolo, M. Durante, C.-A. Reidel, C. Schuy, K. Zink, F. Horst, Frontiers in Physics **8**, 568145 (2020)
8. J. Miller, L. Taylor, C. Zeitlin, L. Heilbronn, S. Guetersloh, M. DiGiuseppe, Y. Iwata, T. Murakami, Radiat. Meas. **44**, 163 (2009)
9. D.J. Thomas, A.V. Alevra, Nucl. Instrum. Meth. A **476**, 12 (2002)
10. A.V. Alevra, D.J. Thomas, Radiat. Prot. Dosim. **107**, 37 (2003)
11. B. Wiegel, A.V. Alevra, Nucl. Instrum. Meth. A **476**, 36 (2002)
12. G. Fehrenbacher, F. Gutermuth, E. Kozlova, T. Radon, R. Schuetz, Radiat. Prot. Dosim. **125**, 209 (2007)
13. D. Boscolo, D. Scognamiglio, F. Horst, U. Weber, C. Schuy, M. Durante, C. La Tessa, E. Kozlova, A. Sokolov, I. Dinescu, T. Radon, D. Radeck, M. Zbořil, Frontiers in Physics **8**, 365 (2020)
14. M. Matzke, Radiat. Prot. Dosim. **107**, 155 (2003)
15. A. Sokolov, E. Kozlova, D. Boscolo, M. Durante, F. Horst, T. Radon, C. Schuy, U. Weber, J. Instrum. **16**, P10022 (2021)
16. T. Nakamura, L. Heilbronn, *Handbook on Secondary Particle Production and Transport by High-Energy Heavy Ions*. World Scientific Publishing Co. Pte. Ltd., ISBN 981-256-558-2 (2006)
17. K. Gunzert-Marx, D. Schardt, R.S. Simon, F. Gutermuth, T. Radon, V. Dangendorf, R. Nolte, Nucl. Instrum. Meth. A **536**, 146 (2005)
18. G. Martino, M. Durante, D. Schardt, Phys. Med. Biol. **55**, 3441 (2010)
19. M. Missiaggia, G. Cartechini, E. Scifoni, M. Rovituso, F. Tommasino, E. Verroi, M. Durante, C. La Tessa, Phys. Med. Biol. **65**, 245024 (2020)
20. S. Bonassi, H. Norppa, M. Ceppi, U. Strömberg, R. Vermeulen, A. Znaor, A. Cebulska-Wasilewska, E. Fabianova, A. Fucic, S. Gundy, I.-L. Hansteen, L.E. Knudsen, J. Lazutka, P. Rossner, R.J. Sram, P. Boffetta, Carcinogenesis **29**, 1178 (2008)
21. T.C. Slaba, I. Plante, A. Ponomarev, Z.S. Patel, M. Hada, Radiat. Res. **194**, 246 (2020)
22. International Atomic Energy Agency: *Cytogenetic Dosimetry: Applications in Preparedness for and Response to Radiation Emergencies*, IAEA Report, Vienna, Austria (2011)
23. R. Lee, S. Sommer, C. Hartel, E. Nasonova, M. Durante, S. Ritter, Mutat. Res. - Gen. Tox. En. **701**, 52 (2010)
24. R.M. Anderson, Clin. Oncol. **31**, 311 (2019)

25. L.C. Paterson, A. Yonkeu, F. Ali, N.D. Priest, D.R. Boreham, C.B. Seymour, F. Norton, R.B. Richardson, Radiat. Res. **195**, 211 (2020)
26. International Commission on Radiological Protection (ICRP): *Recommendations of the International Commission on Radiological Protection,* ICRP Publication 60 (1990)
27. H. Schuhmacher, B.R.L. Siebert, Radiat. Prot. Dosim. **40**, 85 (1992)